ARMY RESEARCH LABORATORY

Development of Thin-film Dye-sensitized Photoactive Materials on Ultra High Molecular Weight Polyethylene (First-year Report)

by Mark H. Griep, Victor Rodriguez-Santiago, Andres A. Bujanda, Josh Martin, Shashi P. Karna, and Daphne D. Pappas

ARL-MR-0813 **April 2012**

Approved for public release, distribution unlimited.

NOTICES

Disclaimers

The findings in this report are not to be construed as an official Department of the Army position unless so designated by other authorized documents.

Citation of manufacturer's or trade names does not constitute an official endorsement or approval of the use thereof.

Destroy this report when it is no longer needed. Do not return it to the originator.

Army Research Laboratory
Adelphi, MD 20783-1197

ARL-MR-0813 **April 2012**

Development of Thin-film Dye-sensitized Photoactive Materials on Ultra High Molecular Weight Polyethylene (First-year Report)

Mark H. Griep, Victor Rodriguez-Santiago, Andres A. Bujanda, Josh Martin, Shashi P. Karna, and Daphne D. Pappas
Weapons and Materials Research Directorate, ARL

Approved for public release; distribution unlimited.

REPORT DOCUMENTATION PAGE

Form Approved
OMB No. 0704-0188

Public reporting burden for this collection of information is estimated to average 1 hour per response, including the time for reviewing instructions, searching existing data sources, gathering and maintaining the data needed, and completing and reviewing the collection information. Send comments regarding this burden estimate or any other aspect of this collection of information, including suggestions for reducing the burden, to Department of Defense, Washington Headquarters Services, Directorate for Information Operations and Reports (0704-0188), 1215 Jefferson Davis Highway, Suite 1204, Arlington, VA 22202-4302. Respondents should be aware that notwithstanding any other provision of law, no person shall be subject to any penalty for failing to comply with a collection of information if it does not display a currently valid OMB control number.
PLEASE DO NOT RETURN YOUR FORM TO THE ABOVE ADDRESS.

1. REPORT DATE *(DD-MM-YYYY)*	2. REPORT TYPE	3. DATES COVERED (From - To)
April 2012	DRI	01-12-2010 to 01-12-2011

4. TITLE AND SUBTITLE
Development of Thin-film Dye-Sensitized Photoactive Materials on Ultra High Molecular Weight Polyethylene (First-year Report)

5a. CONTRACT NUMBER

5b. GRANT NUMBER

5c. PROGRAM ELEMENT NUMBER

6. AUTHOR(S)
Mark Griep, Victor Rodriguez-Santiago, Andres A. Bujanda, Josh Martin, Shashi P. Karna, and Daphne D. Pappas

5d. PROJECT NUMBER
FY11-WMR-063

5e. TASK NUMBER

5f. WORK UNIT NUMBER

7. PERFORMING ORGANIZATION NAME(S) AND ADDRESS(ES)
U.S. Army Research Laboratory
ATTN: RDRL-WM-MA
Aberdeen Proving Ground MD 21005-5069

8. PERFORMING ORGANIZATION REPORT NUMBER
ARL-MR-0813

9. SPONSORING/MONITORING AGENCY NAME(S) AND ADDRESS(ES)

10. SPONSOR/MONITOR'S ACRONYM(S)

11. SPONSOR/MONITOR'S REPORT NUMBER(S)

12. DISTRIBUTION/AVAILABILITY STATEMENT
Approved for public release; distribution unlimited.

13. SUPPLEMENTARY NOTES

14. ABSTRACT
To address Future Force (FF) Soldier power needs and lessen the dependence on cumbersome batteries, flexible dye-sensitized solar cells (DSSC) are an attractive candidate for future solar energy harvesting since they do not require expensive semi-conductor substrates or highly complex processing steps. In this study, the different materials layers comprising the desired DSSC were studied. We used ultra-high molecular weight polyethylene (UHMWPE) as a model substrate, activating UHMWPE surfaces prior to metallization using atmospheric-pressure plasma processing. These surfaces were then used as electrodes. Titania nanotube (TiNT) arrays were prepared by an electrochemical two-step anodization procedure coupled with a rapid inert gas dehydration and ultrasonic agitation detachment method. The free-standing arrays, comprised of hexagonally closed-packed, regularly ordered TiNT membranes, were synthesized and detached from the original Ti substrate. Ruthenium (Ru) and bacteriorhodopsin (bR) dyes were used as active layers. To evaluate the binding of bR dye to the titanium dioxide (TiO_2) versus the commonly used Ru dye, a preliminary test was performed using nanotubes on their original Ti substrate. At 60 mW of illumination, the Ru and bR cells achieved efficiencies at 1.2% and 0.001%, respectively. Although the results are promising, further research efforts are needed to optimize the interfaces between the different layers and improve the performance of the resulting devices.

15. SUBJECT TERMS
Dye-sensitized solar cell, UHMWPE, tunable TiO_2 nanotubes

16. SECURITY CLASSIFICATION OF:			17. LIMITATION OF ABSTRACT	18. NUMBER OF PAGES	19a. NAME OF RESPONSIBLE PERSON
a. REPORT	b. ABSTRACT	c. THIS PAGE			Dr. Mark Griep
Unclassified	Unclassified	Unclassified	UU	42	19b. TELEPHONE NUMBER (*Include area code*) 410-306-4953

Standard Form 298 (Rev. 8/98)
Prescribed by ANSI Std. Z39.18

Contents

List of Figures

List of Tables

Acknowledgments

We wish to thank Dr. Thomas Parker for his help with the sputtering of the titanium (Ti) films, and Daniel Snoha for the x-ray diffraction (XRD) measurements. In addition, we thank Hailey Cramer and Margo Goodall for their research efforts. This research was supported in part by an appointment to the Postgraduate Research Participation Program for Victor Rodriguez-Santiago at the U.S. Army Research Laboratory (ARL) administered by the Oak Ridge Institute for Science and Education through an interagency agreement between the U.S. Department of Energy and ARL. This research was also supported in part by an appointment to the National Research Council Research Associate Program fellowship for Mark Griep.

INTENTIONALLY LEFT BLANK

1. Introduction and Background Information

Soldiers and vehicles, in particular, are constrained by a dependence on bulky batteries to meet their power needs. Future Force Soldiers will be equipped with a wide-array of technology, all requiring electrical power for operation. Integrating solar energy harvesting capabilities with future equipment would relieve the burden of conventional batteries and increase the overall performance of Soldiers. While modern silicon (Si) cells are costly to produce and adversely affect mobility, dye-sensitized solar cells (DSSCs) offer very advantageous properties. These systems are potentially capable of achieving higher efficiencies at much reduced costs, have a lower environmental impact, and are easier to fabricate and manufacture than current Si solutions. Furthermore, their lightweight structure can contribute to a significant reduction of the average equipment weight carried by our Soldiers, thus improving their performance. A considerable improvement of fuel efficiency is also expected when used in ground and aerial military vehicles. Dye-sensitized titanium dioxide (TiO_2) platforms do not require expensive semi-conductor substrates or highly complex processing steps, making roll to roll production possible (*1*). Most importantly, they can be geared to be highly robust and flexible. These attributes qualify DSSCs as an attractive candidate for future solar energy harvesting systems.

The objective of this research is to develop a metalized ultra-high molecular weight polyethylene (UHMWPE)/high-mobility nanomaterials composite for efficient harvesting of solar energy. The envisioned solar harvesting functionality is achieved through a flexible, thin-film multilayered structure, which is deposited on the plasma-modified UHMWPE surface without hindering ballistic functionality or adding significant weight. Research efforts separately explore sensitization efficiency with standard synthetic ruthenium (Ru) dyes and the evolutionary developed retinal protein bacteriorhodopsin (bR).

1.1 DSSC Overview

The classic DSSC is generally composed of a layer of nanocrystalline TiO_2 particles on a conducting substrate, a platinum (Pt) counter electrode, an electrolyte, and an adsorbed Ru-dye as a sensitizer (*2*). The cell presented in this research is unique as it uses TiO_2 nanotubes sensitized with a photoactive protein—bR dye. In contrast to conventional Si systems, where the semiconductor assumes both the light absorption and charge carrier transport, the two functions are separated (*3*). The operating principle is demonstrated in figure 1. An adsorbed dye, which serves as a light absorber and photon to electron converter, is chemically bonded to the surface of titania as shown.

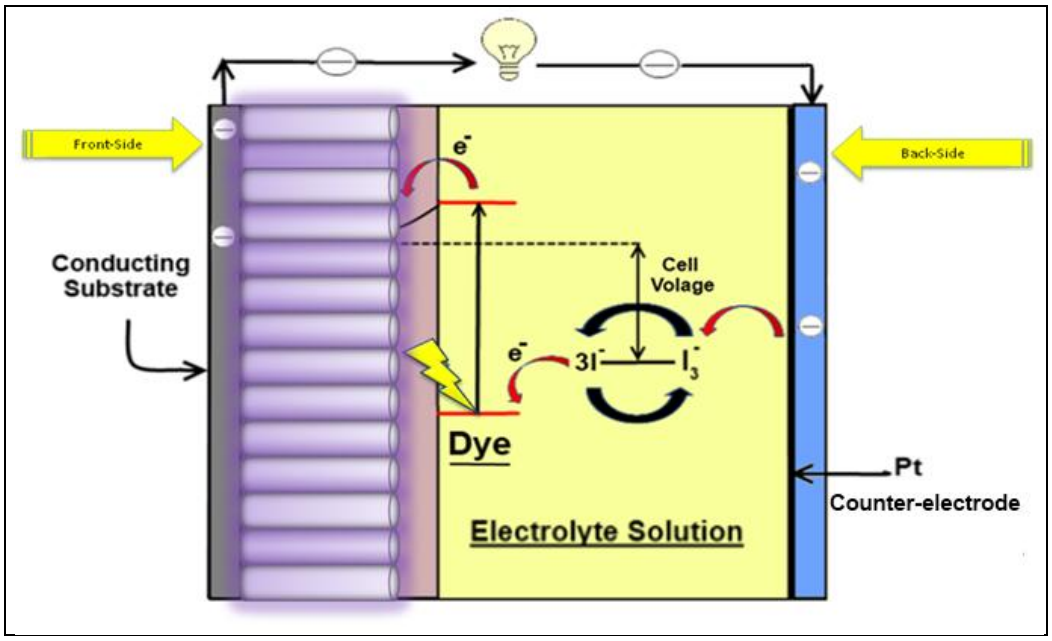

Figure 1. Principle of a DSSC.

A key requirement for the dye is that the lowest unoccupied molecular orbital (LUMO) of the dye molecule is energetically positioned slightly higher than the conduction band of TiO_2. Under the illumination of sunlight, the highest occupied molecular orbital (HOMO)-LUMO transitions in the dye occur. Photo-excitation of the dye leads to rapid injection of electrons into the TiO_2. These electrons are then transferred to the conducting electrode. For typically used Ru dyes, the electron injection from the dye sensitizer to the conduction band of TiO_2 occurs through a metal-to-ligand charge transfer (MLCT) pathway (*4*). Electron donation from the redox couple in the electrolyte, usually an ionic liquid containing an tri-iodide (I_3^-)/iodine (I) system, regenerates the oxidized dye and returns it to its original state. The I_3^- ions formed in the dye regeneration process diffuse through the liquid phase to the cathode, where they are reduced back to I ions to complete the cycle (*5*). The efficiency of collection of the photo-injected electrons, which is a critical factor in device performance, is determined by competition between electron transport to the anode and electron transfer to the I_3^- ions in electrolyte. To date, results of light-to-electricity conversion efficiencies of 11% have been reported in literature (*6*).

While this demonstrates much prospect, the electron transport time in TiO_2 nanoparticles is relatively slow when compared to the rate of de-excitation of the dye and the regeneration time constant of the dye (*7*). Electron flow is slowed down due to defects, surface states, grain boundaries, and other electron trapping sites within the nanoparticles. These factors enhance recombination and adversely affect electron transfer (*8*). In order to minimize this effect, the use of more organized TiO_2 structures, such as nanotubes, have been proposed in recent years (*10*).

TiO_2 nanotubes have a highly ordered structure with vertical pore geometry, which appears to be optimal for the fabrication of solid-state junction cells (*9*). This is due mainly to the one-

dimensional (1-D) conductive path of nanotubes versus the three-dimensional (3-D) unsystematic walk network and grain boundary effects associated with randomly organized nanoparticles, displayed in figure. 2. It has been recently shown that compared to conventional TiO_2 nanoparticle films of the same thickness, aligned TiO_2 nanotube arrays give enhanced light scattering and improved collection efficiencies (*10*). A schematic of a typical DSSC is shown on figure 3.

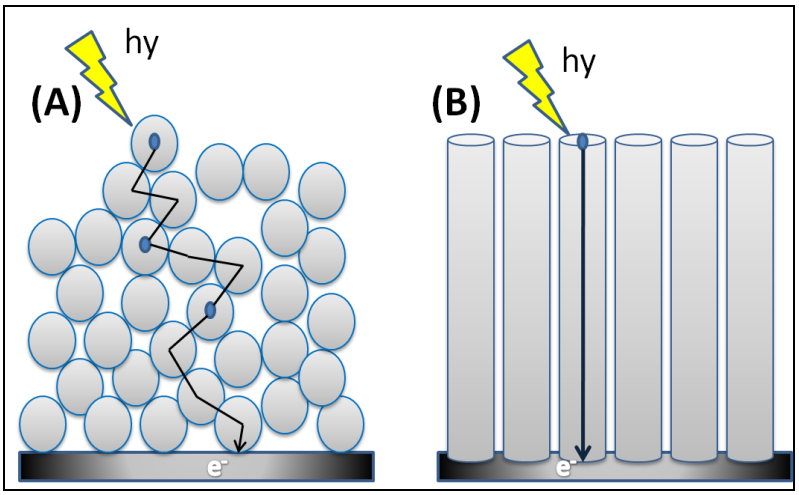

Figure 2. (a) Random electron path thru nanoparticles and (b) direct electron transport in nanotubes.

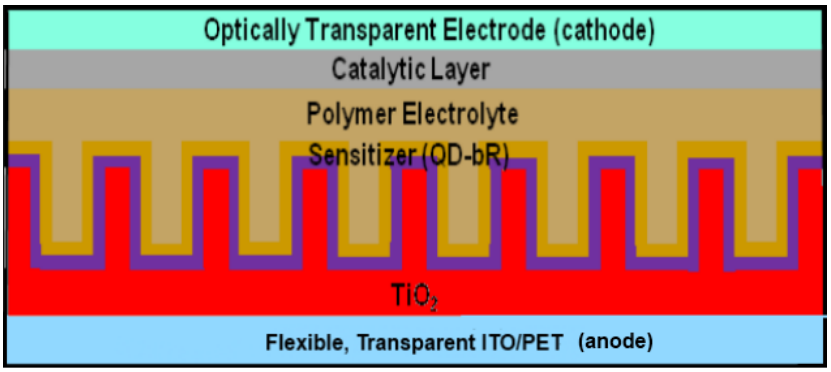

Figure 3. DSSC design.

1.2 Flexible Substrates for DSSC Applications

Flexible solar cells based on plastic substrates are lightweight, thin, and bendable. They can be produced at low cost and can be easily integrated in a curved form, suitable for portable and wearable applications. Flexible substrates require the use of mature low-temperature deposition processes such as sintering, mechanical pressing, hydrothermal crystallization, electrophoretic deposition, or film transfer, among others. Nonetheless, low-temperature treatments usually result in poor material crystallinity and fragile characteristic, possibly limiting the potential of

DSSCs as flexible electronics. Herein lay the challenges and opportunities of flexible substrates for DSSC applications.

1.3 Critical Factors for Efficiency

1.3.1 TiO_2 DSSC Substrates

The conversion efficiency of DSSCs is mainly governed by the following (*11*):

1. molar absorption coefficient and HOMO-LUMO levels of the dye,
2. the effective surface area of the electrodes available for dye anchoring,
3. the transport kinetics of electrons to the substrate,
4. the efficiency of dye regeneration via a redox couple, and
5. the losses arising from recombination and back reactions of injected charge carriers.

Critical optimization factors pertaining to the TiO_2 arrays will be outlined, with a particular focus in maximizing pore diameter to accommodate for the bR dye.

The performance of TiO_2 nanotube (TiNT) arrays in a DSSC as an efficient semi-conductor and electron recipient is directly related to several factors: morphology, crystallinity, and geometry (*2*). A number of studies have been conducted in order to control the dimensions of TiNT arrays via anodic oxidation (anodization). Uniform TiNT arrays with various lengths, diameters, and wall thicknesses can be fabricated in fluoride containing solutions (hydrogen fluoride [HF] and ammonium fluoride [NH_4F]) by tailoring the electrochemical conditions (anodization voltage, fluoride concentration, anodization time, and temperature) (*12–14*).

1.3.1.1 Growth of TiO_2 Nanotube Arrays

The simple electrochemical process of anodizing Ti foils, displayed in figure 4, to produce TiNTs can be accomplished using a two (or three) electrode system with a Ti foil as the working electrode (+), a counter electrode such as Pt (–), and a voltage source. Nanotube formation in fluoride-ion-bearing electrolytes occurs due to three simultaneously occurring processes: electric field assisted oxidation of Ti metal to form TiO_2, the field assisted dissolution of Ti metal ions in the electrolyte, and the chemical dissolution of Ti and TiO_2 due to etching by fluoride ions (which is substantially enhanced by fluoride ions) (*16*). A thin dioxide film develops at the Ti/electrolyte interface due to the following chemical reaction (*10*):

$$Ti + 2H_2O \rightarrow TiO_2 + 4H^+ - 4e^- \quad (1)$$

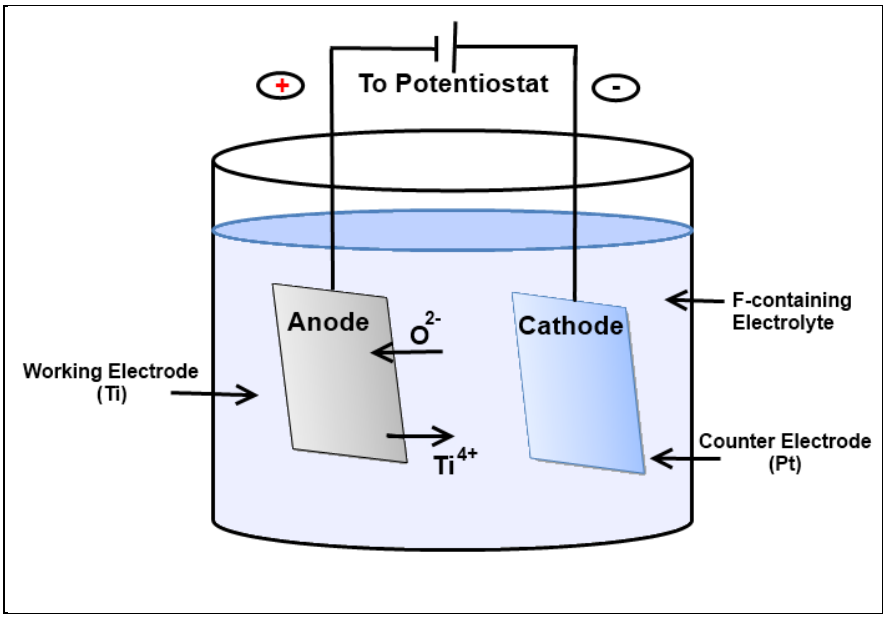

Figure 4. Anodization set up.

As this mechanism occurs, one can note that the current measured will reduce as time goes on. This is due to the increase in resistance provided by the oxide. As the oxygen ions (O^{2-}) are transported from the solution to the titanium (Ti), titanium ions (Ti^{4+}) transported from the titanium to the electrolyte interface are dissolved into the solution. A simultaneous reaction occurs at the TiO_2/electrolyte interface forming soluble fluoride complexes. These create pits at the surface according to the following reaction (*10*):

$$TiO_2 + 6F^- \rightarrow TiF_6^{2-} \quad (2)$$

These complexes dissolve and form pits on the surface of the newly formed TiO_2. As anodization time increases, all three processes continuously increase the depth of the pores (pits) and therefore produce highly ordered nanotubes.

1.3.1.2 Length, Diameter, and Pore Size

Certain geometrical parameters of the nanotube arrays have a large effect on performance. These parameters can be tuned by controlling the anodization conditions. Length, diameter, and pore size (inner diameter) are largely influenced by anodization time, voltage, and NH_4F concentration (*15*). Increasing the overall length of the array allows for more surface area, resulting in more attached dye. The easiest way to modify the length of the array is to increase the anodization time. An increase in the short circuit photocurrent is expected when longer nanotubes are developed due to the increased dye uptake. At the same time, the chance of recombination and electron trapping increases. It has been reported that when the TiNT length is significantly more than 20 µm, the diffusion length of electrons becomes shorter than the length of the tube (*17*). Hence, the photovoltaic (PV) performance shows an initial increase and followed decrease with increasing TiO_2 nanotube length. The same study was able to achieve a

conversion efficiency (Ƞ) of 8.07% using a 20.8-μm nanotube array with an open-circuit voltage (V_{OC}) of 0.814 V, a short-circuit current (J_{SC}) of 15.46 mA cm^{-2}, and a fill factor (FF) of 64.1%. This agrees with other studies that report the maximum internal conversion efficiency is achieved for tubes of a length of approximately 20 μm (*2*).

In order to further modify the dye "absorbing" capabilities of the nanotubes, diameter and pore size are very important. These factors are critical depending on certain situations. In order to take full advantage of nanotubes having both inner and outer walls, the dye being used must also fit inside the inner diameter. According to Schmuki's studies, the diameter of the tubes can be adjusted by the anodization voltage (*9*). In addition, modifying the concentration of the electrolyte used during anodization further modifies the pore diameter and wall thickness. This occurs due to the increase in the dissolution rate, which increases due to a higher amount of fluorine ions (F^-) within the electrolyte solution, leading to an increase of the inner diameter - thus reducing wall thickness and increasing the pore size (*10*).

1.3.1.3 Crystalline Structure

The crystal structure of TiO_2 tube walls is a significant factor affecting its electronic properties. When anodically formed, the TiO_2 arrays are initially in an amorphous state. Due to a large amount of defects, impurities, and other recombination sites, the amorphous TiO_2 has hardly any conversion efficiency (*11*). In order to harness the maximum potential of the TiNT array, the nanotubes must be annealed to a crystallite form.

When annealed at temperatures between 300 and 500 °C for about 3 h, the anatase crystalline form of TiO_2 can be obtained. At higher temperatures, 550 °C and above, rutile-based TiO_2 will begin to develop. In addition to annealing temperature, the ramping speed has an effect on solar cell performance (*2*). High ramping speeds (greater than 30 °C/min) can adversely affect performance due to an increase in structure defects.

Little attention has been paid to the rutile form of TiO_2, although it is used as a base in most paints due to its light scattering ability. In general, a pure anatase TiO_2 nanostructure is preferred over rutile due to its superior performance in DSSCs. This results from its surface chemistry and potentially higher conduction-band energy (*18*). Rutile films consist of homogenously distributed rod-shaped particles. These particles show no preferred orientation and therefore have a much smaller packing density compared to anatase-based particles. The smaller packing density results in smaller particle connectivity. In other words, electrons move slower through rutile-based TiO_2 than in anatase-based structure. In addition, anatase arrays have a larger surface area per unit volume (about 25%); this allows for more dye to be absorbed. As a result, anatase structures can achieve a 30% higher J_{SC} than rutile. Maintaining a pure anatase TiO_2 nanostructure is essential for achieving a high efficiency DSSC using nanotubes.

2. Materials and Experimental Procedure

2.1 Functionalization of Ultra High Molecular Weight Polyethylene

2.1.1 Plasma Treatment

The plasma system used in these experiments was an atmospheric plasma system (APC) 2000 from Sigma Technologies Intl. Inc. The system uses a cylindrical roller configuration and it is operated in an open atmosphere setup, as shown in figure 5. The roller serves as the ground electrode and it is covered with aluminum oxide (Al_2O_3) as the dielectric material. Two high-voltage electrodes are positioned on top of the roller at a distance of 2 mm and have slit channels to allow gas diffusion. The flow rate for the carrier gas, in this case, helium (He), was 200 $cm^3\ s^{-1}$, and it was equally divided with one line going directly to one of the electrodes (#2), and another leading to electrode #1 through an evaporator. The latter was used to supply the reactive gas, in this case water vapor (figure 5). The amount of water vapor entrained in the He gas stream can be controlled by changing the temperature and flow of the carrier gas in the evaporator. In this study, the temperature of the evaporator was kept at 25 °C, which provided a water vapor mass fraction of 65.2 mg/g of gas mixture. For these experiments, one electrode (#2) was used for pre-treatment using the carrier gas (He) and the other electrode (#1) was used for functionalization purposes using the reactive gas (water vapor). A radio-frequency power supply operating at 90 kHz was used, with power densities ranging between 0.86–2.58 W cm^{-2} leading to the ignition of an electrical discharge known as dielectric barrier discharge (DBD), since one of the metal electrodes is covered by a dielectric material. Under these conditions, the generated plasma was mostly uniform; however, the presence of microdischarges was inevitable. Samples were mounted on the rotating cylindrical dielectric surface and the plasma exposure time was varied by changing the rotating speed of the roller. Plasma exposure times ranged from 0.4–40 s.

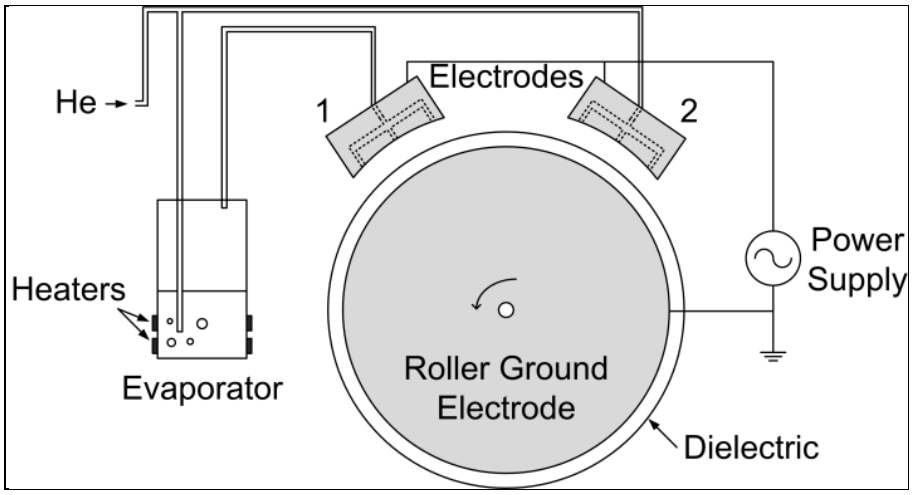

Figure 5. Schematic of the atmospheric plasma system.

2.1.2 Materials

UHMWPE films (Goodfellow) with thickness of 75 μm, were cut into 2.5 × 5 cm strips. The samples were rinsed with ethanol to remove surface residual contamination and were let to dry in air prior to plasma exposure.

2.1.3 Surface Characterization Techniques

Wettability testing was carried out using a static contact angle setup using the sessile drop method. The setup consists of a 100-μL syringe held in place above a moveable stage. Contact angles were recorded using a goniometer equipped with a charge-coupled device (CCD) camera and an image capture program employing LabVIEW software (National Instruments, USA). Small strips (5 x 1 cm) of the sample film were cut and then placed onto a glass microscope slide using double-sided tape to ensure a flat viewing surface. The glass slide is then placed onto a stage, where a 5-μL deionized water drop is dispensed from the syringe onto the film surface. The drop is allowed to reach equilibrium prior to recording the measurement and before evaporation occurs. Six to ten drops were used for each sample, and the values were averages to obtain final contact angle value.

Near-surface compositional depth profiling was performed using the Kratos Axis Ultra X-ray photoelectron spectroscopy (XPS) system, equipped with a hemispherical analyzer. A 100-W monochromatic aluminum (Al) Kα (1486.7 eV) beam irradiated a 1 mm × 0.5 mm sampling area with a take-off angle of 90°. The pressure in the XPS chamber was held between 10^{-9} and 10^{-10} Torr. Elemental high resolution scans for C1s, F 1s, and O1s were taken in the constant analyzer energy mode with a 20-eV pass energy. The calibration energy for the hydrocarbon C1s core level was assigned a value of 285.0 eV for the binding energy scale.

Morphological changes of plasma treated surfaces were observed using scanning electron microscopy (SEM). A field emission SEM (Hitachi, model S4700) was used in secondary electron mode, using mixed of upper and lower detectors. The magnification ranged from 2500× up to 100,000× and the working distance varied from 3 to 9 mm. Samples were stored in a dry box in order to limit exposure to moisture and other contaminants. Several areas on each sample were investigated in order to discern the uniformity of the untreated and plasma treated surfaces.

2.2 Wide Band Gap Semiconductor Substrate Preparation

2.2.1 TiO_2 Nanotubes Preparation and Deposition

The conversion efficiency of DSSCs is mainly governed by (1) molar absorption coefficient and HOMO-LUMO levels of the dye, (2) the effective surface area of the electrodes available for dye anchoring, and (3) TiO_2 nanotube arrays were grown using a single-step anodization process. Ti foils (Sigma-Aldrich, 99.7%, 0.25μm) were electrochemically anodized in a standard two-electrode cell using a Pt counter-electrode and an Agilent E3649A DC power supply. The electrodes were kept at a fixed distance of 1.5 cm. The foils were first mechanically polished

using a 9-µm diamond compound with a silk cloth and microid extender followed by colloidal silica/wetted imperial cloth. The foil was then cut into 1 cm x 2 cm samples. Then, the substrates were separately sonicated in acetone, isopropanol and ethanol, each for 5 min before, being rinsed with deionized (DI) water. The anodization process was performed at 60 V for 2–6 h using an electrolyte consisting of 0.25 wt.% NH_4F and 0.75% H_2O in ethylene glycol. The anodized samples were rinsed with DI water and then soaked in methanol for 30 s to initiate the detachment procedure. Free-standing TiNT membranes were separated from the Ti substrate by drying the methanol-wetted samples with a stream of nitrogen (N_2) gas. This caused the freshly formed TiNT array to rapidly dry and delaminate from the substrate. To effectively remove the TiNT membranes; methanol wetting and N_2 blowing were repeated several times.

To crystallize the amorphous TiNT arrays into the anatase phase, a single-step annealing process was used. The TiNT arrays were heated in a tube furnace at 450 °C for 3 h using a heating rate of 20 °C s^{-1}. After annealing, the arrays are to be bonded to a polyethylene terephthalate (PET) film using a TiO_2 solution containing titanium butoxide and polyethylene glycol and sintered at a low temperature of 200 °C to keep the PET from thermally degrading.

Following the annealing process, the TiNT/PET films are to be sensitized using a bR dye for 16 h. Due to time constraints, among other obstacles, the performance of a DSSC sensitized with bR is evaluated on a Ti substrate rather than a flexible indium tin oxide (ITO)/PET film.

2.2.2 TiO_2 Nanoparticle Preparation and Deposition

The TiO_2 solution was prepared in an acetic acid solution (10% by weight) by slowly adding 2 g of TiO_2 (P25) nanoparticles in 3.2 g of acetic acid solution on a magnetic stirring hot plate with a stirrer. Next, 0.3 g of ethanol was added to help with viscosity and the solution was then sonicated for 20 min. Then, 0.3 g of polyethylene glycol (PEG) (MW=200) was added to help with porosity. Lastly, the solution was stirred for 10 min, sonicated for 15 min, and then stirred overnight to insure a uniform solution. After producing a well-mixed TiO_2 solution, 0.1%, 0.5%, and 1% of pristine graphene was added to each solution. The solution was then stirred for 15 min and then sonicated for 20 min. Before depositing the solution onto the fluorine-doped tin oxide (FTO) coated glass substrate, the solution was stirred for an additional 10 min to insure a uniform solution before deposition. Prepared solutions were stored in a dark environment at room temperature. Immediately before use, solutions were water-sonicated for 10 min and then stirred with a magnetic stirrer at room temperature for 10–30 min.

The experimental substrates were 25 mm x 25 mm x 1 mm samples of FTO glass and 25 mm x 25 mm samples of ITO-PET cut from a sheet. Films were deposited onto the substrates via doctor blade. The substrate was secured and framed with two pieces of scotch tape, creating a channel on the surface ~15 mm wide and 40–50 µm deep. A few drops of solution were dropped in the channel with a pipette and spread evenly with a glass rod. The resulting film was air dried for 10 min, and then the tape was removed. The samples were then immediately subjected to annealing treatments of 450 and 150 °C for the FTO glass and ITO-PET, respectively.

2.3 Preparation of Photosensitive Dyes

The final step of the DSSC electrode preparation is the attachment of the photosensitive dye to the TiO_2 electrode. Once annealed and cooled, the prepared TiO_2 electrode is immersed in the desired photosensitive dye solution to achieve maximal dye loading.

2.3.1 Synthetic Ruthenium Dyes

A synthetic Ru dye solution was produced according to standard procedures. Ru-N719, which is the dye standard in DSSC test designs, was purchased from Sigma Aldrich and applied without further purification. The dye solution was created by adding 3.566 mg of Ru-N719 to 10 mL of ethanol and sonicated until thoroughly mixed. The solution is kept in an optically opaque jar for storage and application to prevent photobleaching.

2.3.2 Bacteriorhodopsin Protein Sensitizer

For engineered applications, bR is processed into membrane patches, known as purple membrane (PM). A PM is simply a large cell membrane patch, on average 500 nm in diameter, which is composed of multiple bR molecules and their associated lipids. It is called PM due to its distinct purple color, which is due to the absorption properties of the bR molecules. The highly purified bR used in this work was attained from the Michigan Technological University.

2.4 Construction and Testing of DSSC

The DSSC requires an electrolyte material to complete the circuit between the photoanode and counter electrode, which is typically achieved with an I/I_3^- electrolyte mixture. This work used a lithium iodide (LiI) electrolyte prepared with 3.346 g of LiI, 634.522 mg of I_2, and 4.056 g of 4-tert-butylpyridine mixed in 50 mL of acetonitrile. Acetonitrile was chosen as the solvent due to its benefits in regard to the I/I_3^- solution (*3*). To fabricate the solar cell, the TiO_2 solution was doctor bladed onto the FTO-coated glass substrate and sintered at 450 °C for 30 min with a ramp speed of 20 °C/min. This allows the solution to turn into a crystalline structure. Then, this TiO_2 photoanode was soaked in a 0.3-mM dye solution overnight (~18 h) and subsequently rinsed with ethanol and dried with nitrogen. The reference Pt counter electrode was produced by sputter deposition onto an FTO-coated glass substrate and had an approximate thickness of 50 nm. Then, a chemically inert sealant was used to seal both electrodes together while allowing enough space between the electrodes for 10 µL of electrolyte to be added through a 1-mm-diameter hole in the counter electrode. An additional hole was drilled to allow for air to escape when electrolyte was added. Following the insertion of the electrolyte, the holes were sealed with an inert Kapton tape to ensure no leaks are present. Copper tape and a blocking mask were also applied to promote conductivity and control of the irradiated area, respectively.

Efficiency measurements were made by recording the current-voltage (I-V) values to determine the maximum output power and cell efficiencies. I-V measurements were conducted using a Keithley 6430 Sourcemeter under air mass (AM) 1.5 (100 m Wcm^{-2}) illumination provided by a 150-W xenon lamp.

3. Results and Discussion

3.1 Plasma Modification of UHMWPE

3.1.1 Contact angle of Plasma Treated Surfaces

Water contact angle (WCA) measurements as a function of plasma treatment time for UHMWPE are presented in figure 6. Surface modification occurs within fractions of a second of plasma exposure with WCA decreasing by 36% for UHMWPE after only 0.4 s of treatment in He-water vapor plasmas operated under atmospheric pressure conditions. After approximately 6 s of exposure, all polymers reached their lowest WCA with no appreciable change up to 40 s of exposure. The maximum recorded WCA decrease was 59%. The final WCA for UHMWPE, treated with He/H_2O plasma, were at least 10 °C lower than similar experiments performed in the past with He/O_2 plasmas at the U.S. Army Research Laboratory (ARL) (*19*). The WCA data can be fitted to an exponential decay function (figure 6) in the following manner:

$$\frac{c(t)-c(t_\infty)}{c(t_0)-c(t_\infty)} = \exp(-kt), \tag{2}$$

where $c(t_0)$ is the WCA for the untreated sample, $c(t)$ is the contact angle of the sample at any given exposure time, $c(t_\infty)$ is the contact angle after maximum plasma exposure, and k can be interpreted as a rate constant for the surface functionalization reaction. The value of k from the fit was 1.6 s^{-1} for UHMWPE. The use of water vapor-based atmospheric DBDs has many advantages over other gases due to its abundance and low cost. The wettability improvement of various polymers including UHMWPE, PET and polytetrafluoroethylene (PTFE) using air dielectric barrier discharges has been studied in the literature (*20*, *21*). However, the reported WCAs appear to be higher than those observed in our study and also require longer exposure time.

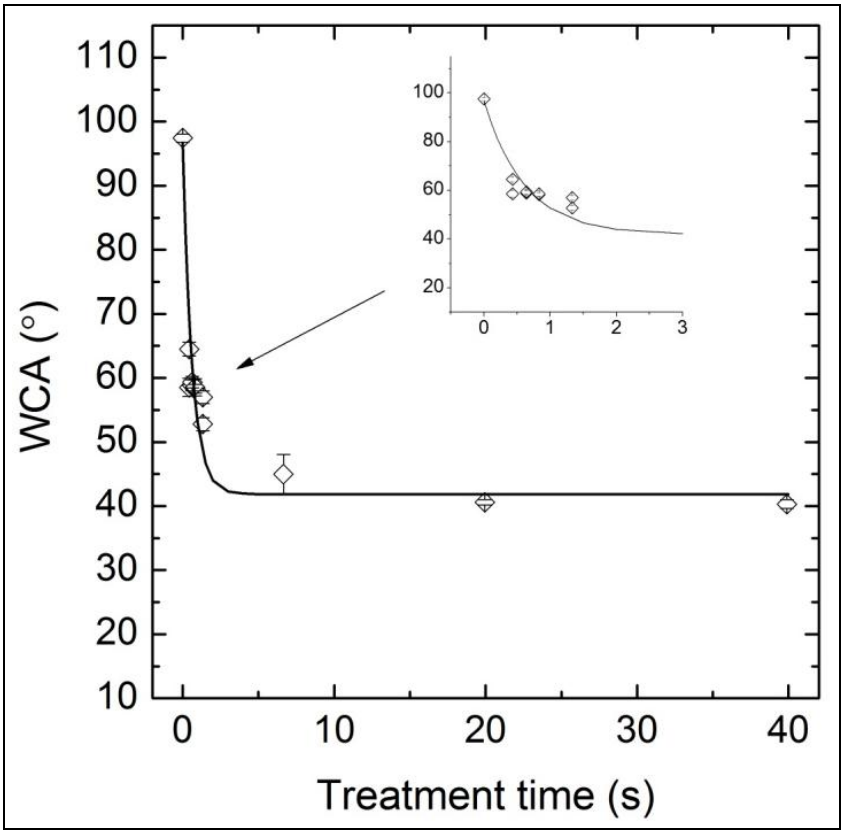

Figure 6. WCA of polyethylene films treated with He/H_2O plasma. The inset shows WCA values for treatment times less than 2 s.

3.1.2 XPS Analysis

XPS analysis of the polymers was performed on samples after exposure to the plasma for 0.43, 0.64, 0.83, 1.33, and 15 s; and the results were compared to those obtained for the as-received material. Figure 7 shows the XPS spectra of the carbon (C 1s) peak for untreated and plasma treated UHMWPE. The untreated sample (figure 7a) shows a single peak centered at 285.0 eV, which corresponds to the aliphatic carbons, C – C. After plasma treatment for 15 s, several C-O peaks appear (figure 7b) at higher binding energies, adding a tail to the single peak observed for the as-received film. C 1s and O 1s peak assignments for UHMWPE are shown in table 1 (*22*). The appearance of surface oxidation is clear even for short plasma exposure times. After 15 s of plasma exposure, carboxylic acid groups dominate the surface chemistry followed by hydroxyl and carbonyl groups, respectively. The total atomic oxygen surface concentration for UHMWPE after 15 s of plasma exposure was close to 26%. A mechanism for the functionalization of polyethylene under atmospheric pressure oxygen plasma has been proposed in the literature (*23*) and it should be similar in the case of water vapor plasma, where hydroxyl radicals are the predominant species. XPS results reveal that the activation of UHMWPE begins with the hydrogen abstraction, and therefore, the formation of active sites at the polymer backbone. This is followed by the incorporation of hydroxyl radicals at the active sites, which dominate the bulk plasma phase in water vapor dielectric barrier discharges. Next, further addition of hydroxyl

groups will generate two parallel reaction paths: (1) chain scission to form carboxylic acid groups and (2) release of water molecules to form carbonyl groups. The latter reaction path appears to be less favorable since it has the lowest contribution at all plasma treatment times.

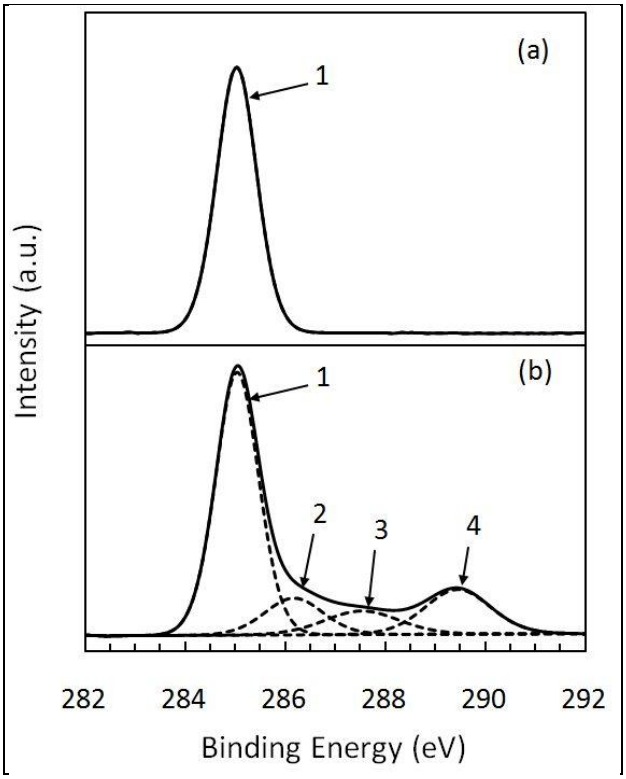

Figure 7. XPS spectra for the C 1s peak for (a) control and (b) He-H_2O plasma treated UHMWPE.

Table 1. C 1s and O 1s XPS peak assignments for the plasma treated UHMWPE.

Peak	Peak no.	Binding Energy (eV)	Assignment
UHMWPE			
C 1s	1	285.0	C – H, C – C
	2	286.5	C – O(H)
	3	287.5	C = O
	4	289.0	(C = O) – OH
O 1s	1	532.2	C = O
	2	533.7	C – O(H)

The preceding analysis demonstrates that the wettability improvement; therefore, the increase in surface energy of the polymer surface by plasma treatment should provide a favorable environment for the increased adhesion of a metal layer deposited on the surface and was the reason for performing the plasma activation step.

3.1.3 Metallization of UHMWPE

UHMWPE samples were metalized under vacuum using a custom built sputtering system (Kurt Lesker). Ti was deposited on the plasma-treated UHMWPE films with a target thickness of 120 nm. Figure 8 shows an SEM image of the metalized surface.

From the image, it can be seen that the coating is uniform and conformal showing minimal cracks. The continuity of the film was tested with a digital multimeter at different locations on the sample.

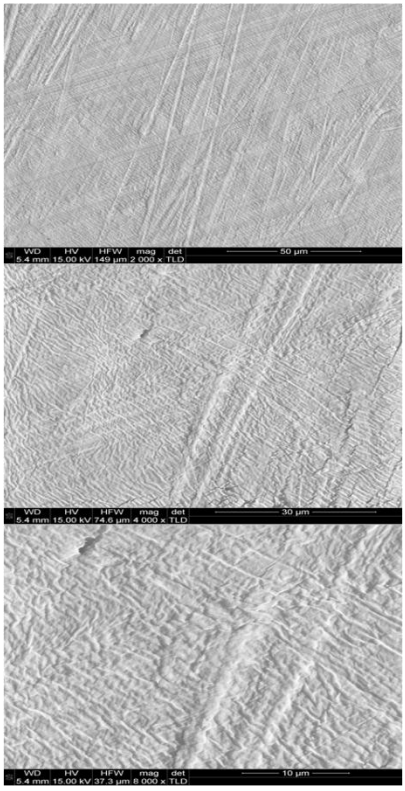

Figure 8. SEM image of the metalized surface of plasma-treated UHMWPE at different magnifications: (a) 2000×, (b) 4000×, and (c) 8000×.

3.2 TiO_2 Nanoparticle DSSCs

Titania nanoparticle substrates were prepared with P25 Degussa particles using the described doctor-blade method, as opposed to spin-coating and airspray techniques, which showed greatly decreased energy harvesting efficiencies. SEM images of the FTO glass and the prepared TiO_2 nanoparticle substrates are shown in figures 9 and 10, respectively. Output of the prepared DSSC device when sensitized with natural anthocyanin dyes is shown in figure 11.

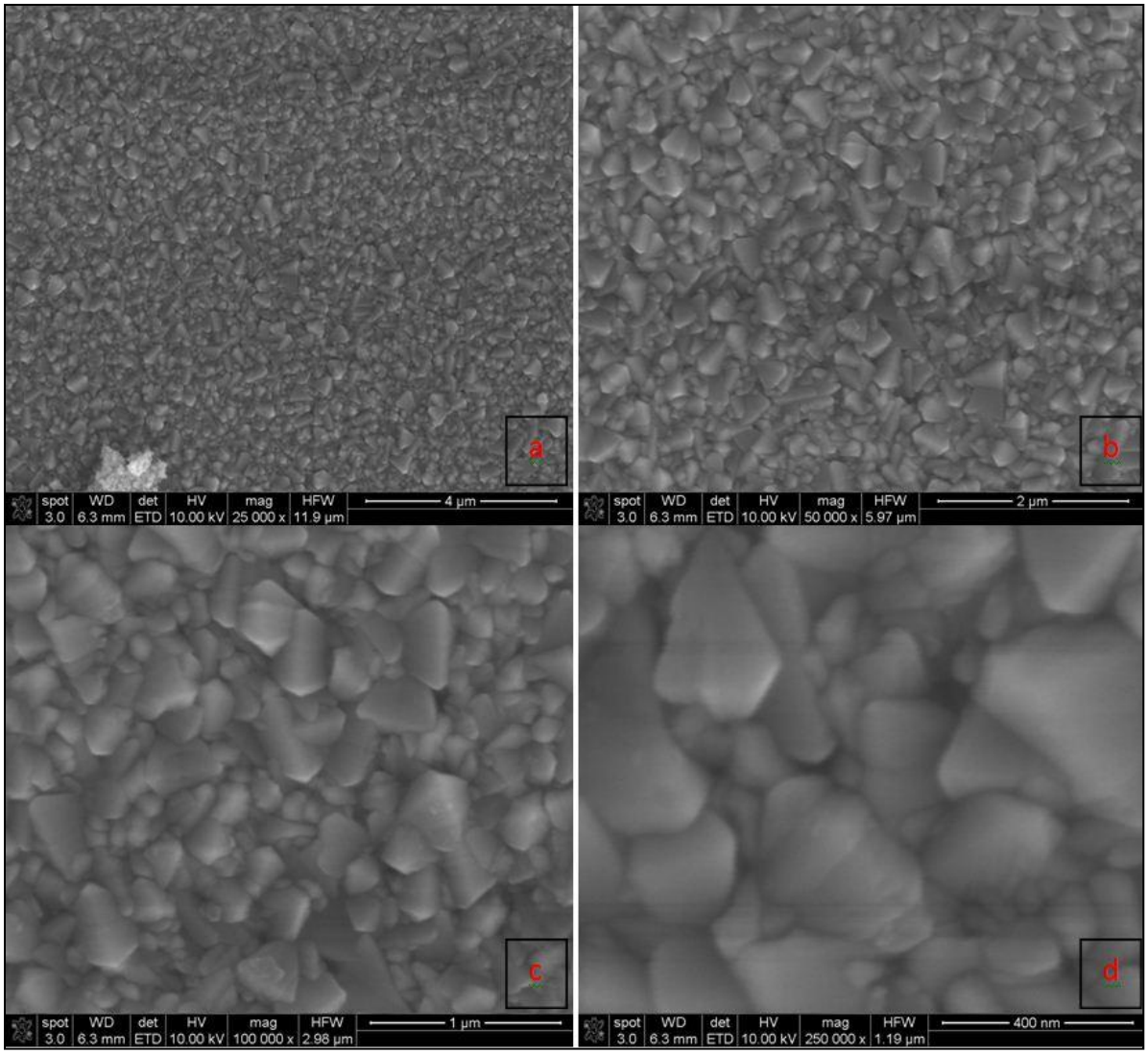

Figures 9. SEM images of FTO glass substrate from doctor blade method at (a) 25000×, (b) 50000×, (c) 100000×, and (d) 250000× magnifications

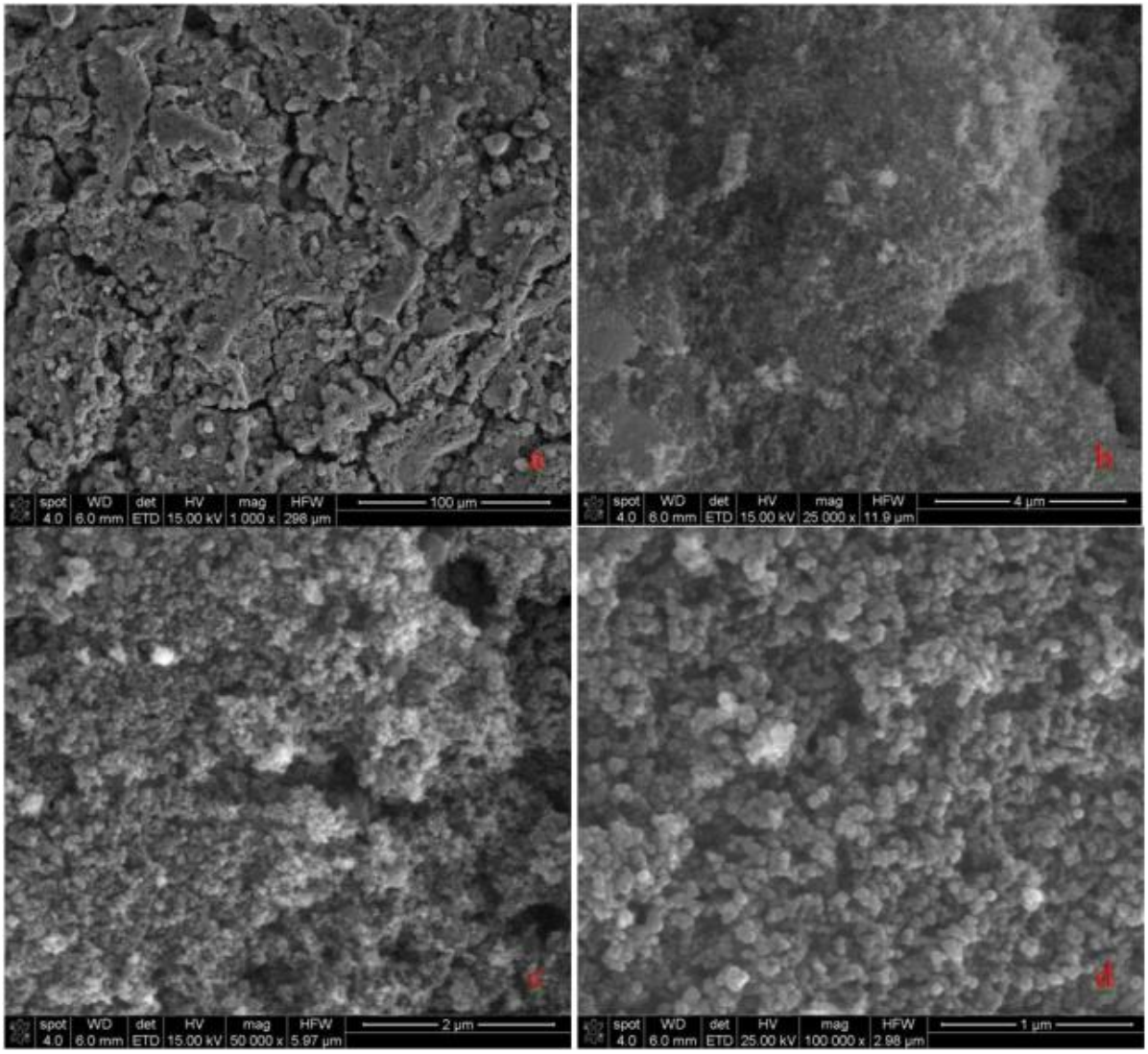

Figures 10. SEM images of FTO glass substrate from doctor blade deposition method at (a) 1000×, (b) 25000×, (c) 50000×, and (d) 100000× magnifications

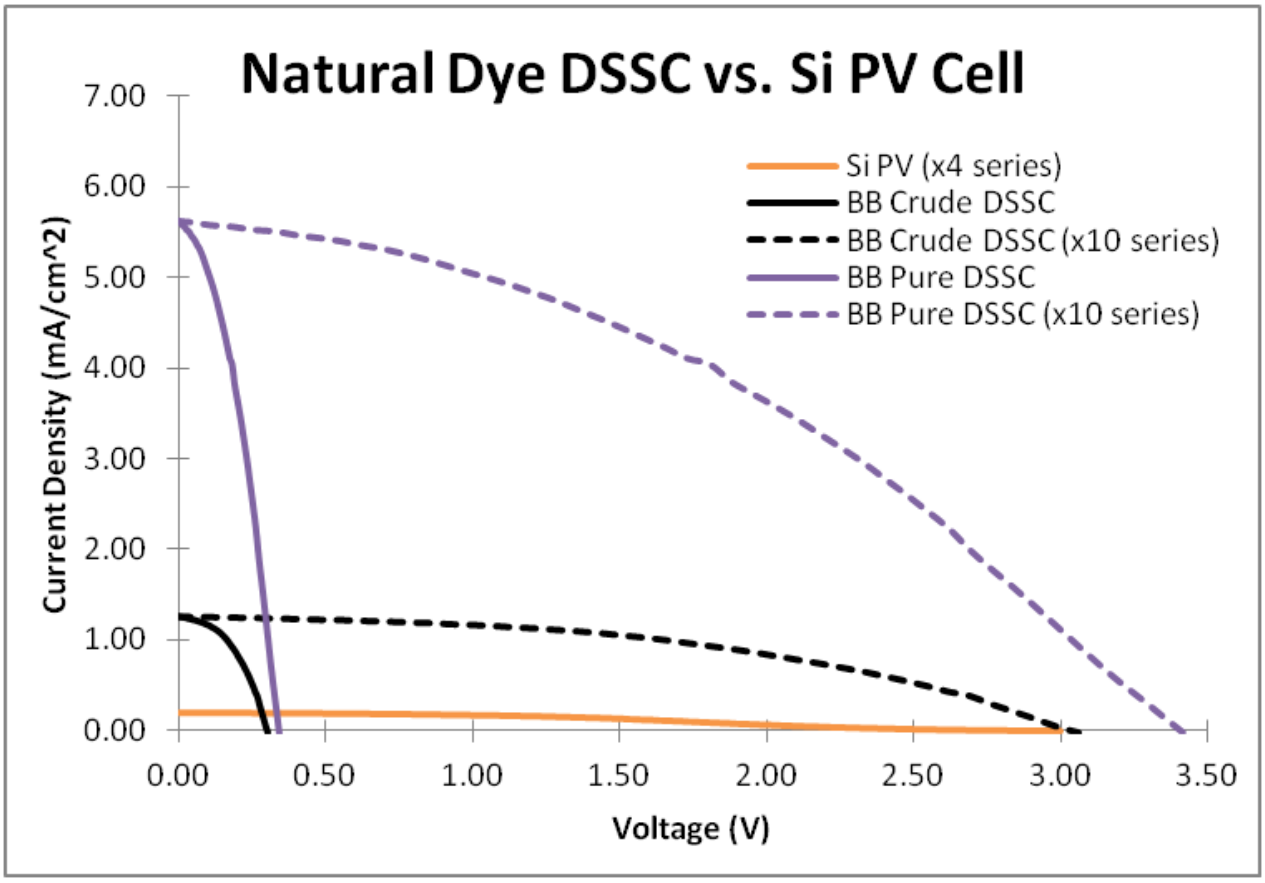

Figure 11. PV output of TiO2 NP DSSC.

As shown in figure 11, a highly packed nanoparticle surface is created to maximize dye adsorption surface area. After dye adsorption the PV output was measured at 100 mW/cm^2 input power, as shown in figure 18. Cells were created with varying forms of the photosensitized anthocyanin and compared against a simple Si PV cell, which had active areas of 0.25 and 2.5 cm^2, respectively. Output for the cell yielded a 0.70% efficiency for the purified anthocyanin dye, with a short-circuit current density far exceeding that of the Si PV cell. The DSSC device falls short of the Si cell in open-circuit voltage; however, this can be compensated by wiring the DSSC devices in series. Figure 11 demonstrates the theoretical output of 10 DSSCs wired in series, yielding the same active area as the Si PV cell. This extrapolation demonstrates the applicability of DSSC devices compared to amorphous Si PV cells in low voltage applications.

3.3 TiO_2 Nanotube DSSCs

Figure 12 shows the effects of methanol wetting and N_2 blowing on freshly anodized TiNT arrays. Due to the low surface-tension of methanol, soaking the TiNT arrays allows the methanol to penetrate the oxidized layer and aids in the delamination of the nanotube layer. This resulted in a nanotube array nearly twice the size of one collected without methanol wetting.

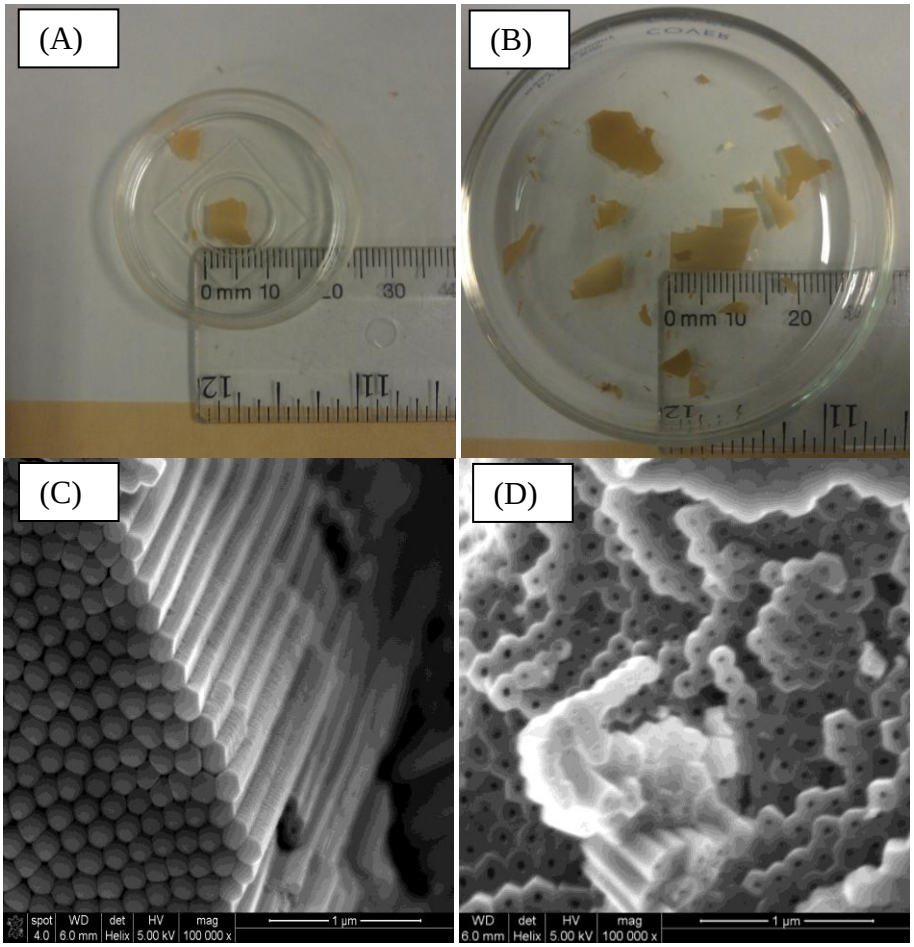

Figure 12. (a) Without methanol wetting, (b) with methanol wetting, (c) side SEM view of the hexagonal, highly oriented nanotube array, and (d) top view.

SEM images in figure 12 (c and d) show highly aligned, densely packed, hexagonally oriented nanotube arrays. This result was surprisingly unexpected, because the arrays were formed using a single step anodization procedure. Figure 13 reveals that the hexagonally aligned nanotubes also exhibit bamboo-like rings. Although this has been seen before, the standards in literature believe these rings are formed by alternating (or stepping) the applied voltage. However, these highly organized arrays were anodized at a constant 60 V for 3 h.

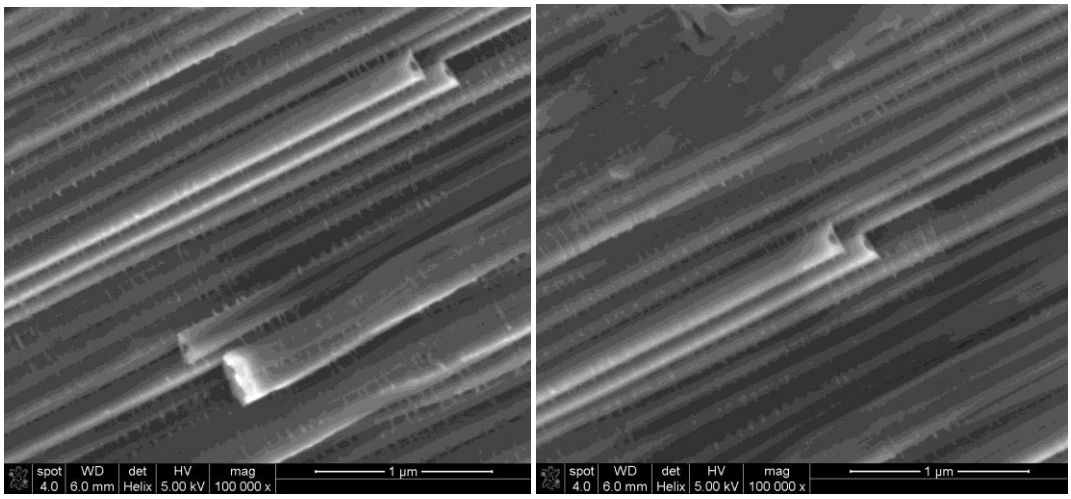

Figure 13. SEM Images of TiO_2 nanotubes anodized at a 60 V for 3 h, revealing bamboo-like rings.

These structures are unique from commonly anodized nanotubes because of the bamboo-like ring formations, which seem to be growing very uniformly. Although they may not occur at fixed distances along the tubes, one can note that the rings are forming in distinct, homogeneous layers. These rings may contribute to the highly aligned and close-packed nature of the array. The nanotubes shown in figure 13 have a length of 19 µm, tube thickness of 64 nm, and a pore diameter of 32 nm. Since this was made immediately after mixing a batch of electrolyte solution (0.25 wt.% NH_4F and 0.75 wt.% H_2O in ethylene glycol), it is possible that the NH_4F was not equally distributed. The opposite affect can be seen in figure 14, in which the uneven distribution of NH_4F right after mixing a batch of electrolyte solution resulted in extraordinarily high concentration of F^- and the complete dissolution of the Ti electrode. The high wall thickness compared to pore size is most likely due to a low concentration of F^- ions in the electrolyte solution, which slowed down the dissolution rate, thus decreasing the inner diameter. Therefore, by increasing the concentration of F^- ions in the electrolyte from 0.25 to 0.75 wt.%, the inner diameter can be increased from 32 to 130 nm, as shown in figure 15. The structures on the surface of the tube result from bR dye soaking.

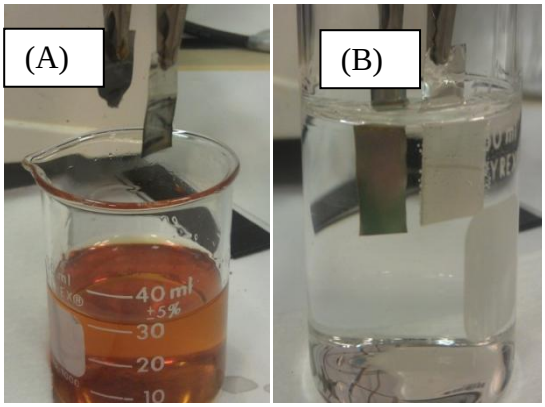

Figure 14. (a) Anodization with a high NH_4F concentration (>1%) and (b) anodization with a normal NH_4F concentration (0.25%–1%)

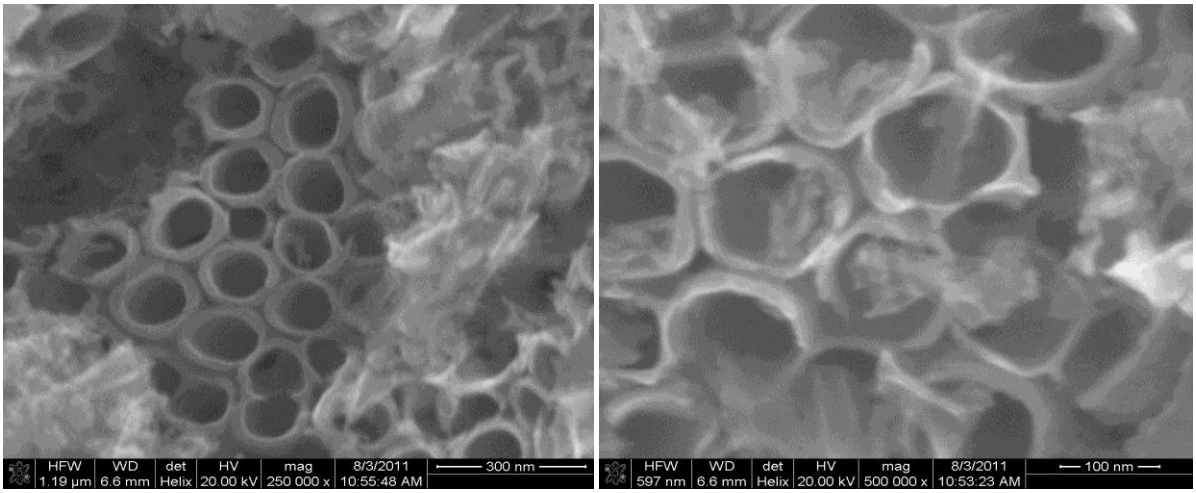

Figure 15. SEM images of nanotubes anodized at 60 V with 0.75 wt.% of NH_4F after bR soaking.

Further investigation of the effects of anodization parameters show that nanotube arrays can be over-anodized. The SEM images in figure 16 report samples that were anodized for 6 h at 60 V, using an electrolyte consisting of 1 wt.% NH_4F and 0.25 wt.% H_2O. This shows the effects of electrode preparation as well as the sensitivity of the nanotubes. The SEM images report grass-like structures, also known as nanowires, of approximately 24 nm thickness sitting on top of a highly porous honeycomb-like nanostructure with wall thickness of only 36 nm. The "nanograss" is most likely the result of not mechanically polishing and sonicating the electrode prior to anodization. This coupled with a higher concentration allowed an accelerated chemical attack on the tube ends and the formation of nanograss. The top surface was left non-uniform due to an uneven dissolution of the Ti. The longer anodization time presumably also contributed to the rapid breakdown of the nanotubes.

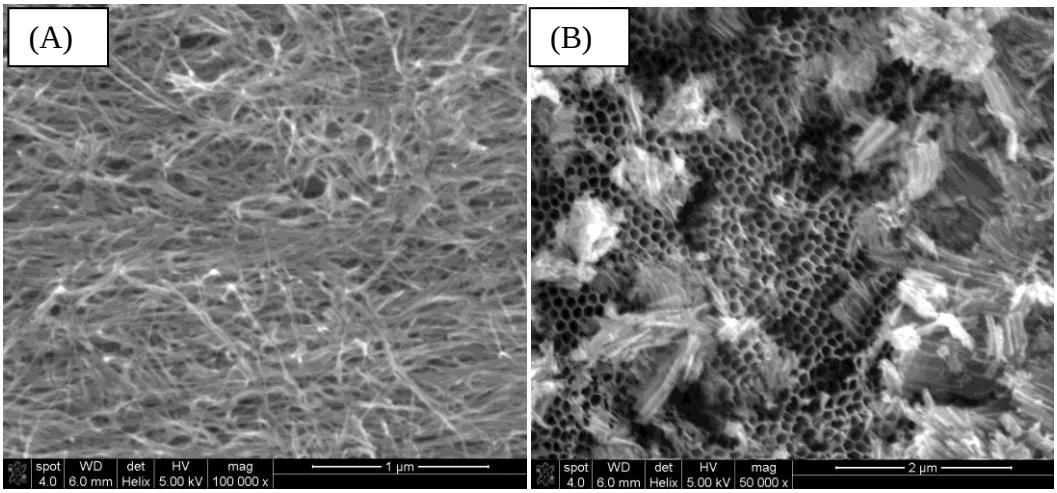

Figure 16. (a) Nanograss formations and (b) honeycomb structure anodized at 60 V for 6 h at a 1 wt.% NH_4F concentration.

X-ray diffraction (XRD) analysis, shown in figure 17, agrees with the TiO_2 phase diagram and verifies the standard in literature that states annealing TiO_2 arrays at 450 °C at for 3 h will achieve a pure anatase structure. This is a critical step in achieving the maximal electron transport capabilities of the nanotubes.

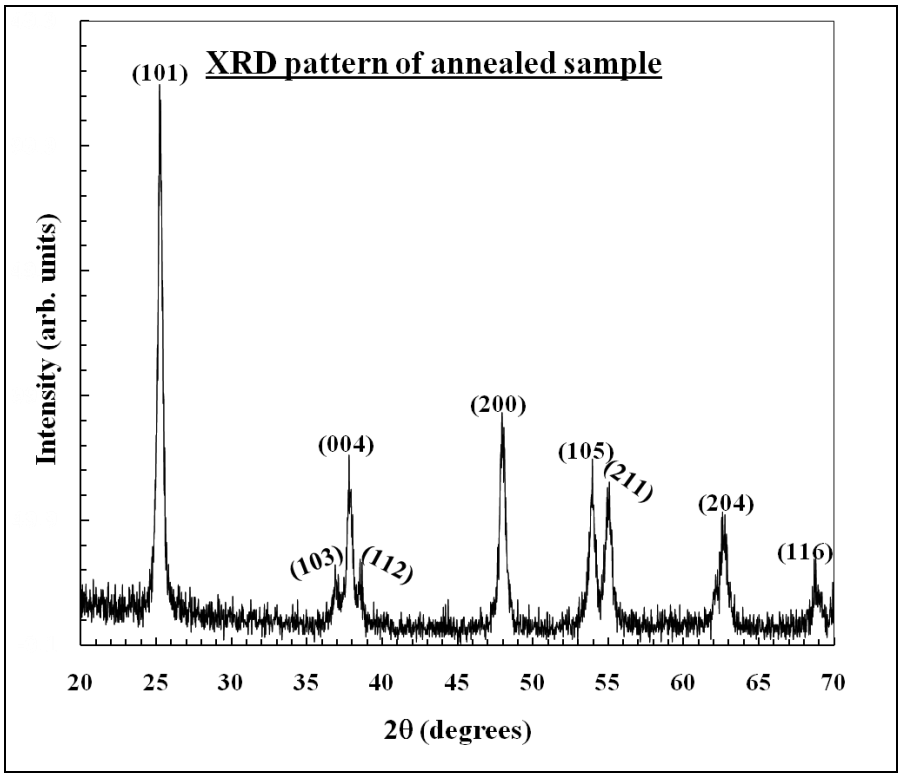

Figure 17. XRD measurement of TiO_2 nanotubes annealed at 450 °C.

Figure 18 displays voltage versus current density readings of nanotube DSSCs. In order to evaluate the binding of bR-dye to the TiO_2 versus the commonly used Ru-dye, a preliminary test was performed using nanotubes on their original Ti substrate. Using a Newport illuminator (model 67005) and a Keithley 6430 SourceMeter, I-V measurements were taken. The efficiency of the cells was determined by dividing the max power output of the cell by the input power from the illuminator. At 60 mW of illumination, the Ru and bR cells achieved efficiencies at 1.2% and 0.001%, respectively (although the current density, voltage, and overall efficiency were fairly low). This is expected because of a thin TiO_2 layer that forms between the Ti substrate and the nanotubes array, which adversely affects the cells performance. The cell must also be illuminated through the counter electrode because Ti is opaque, heavily reducing the amount of photons that make it to the photoanode. Furthermore, it is likely that the bR molecules were too large to effectively bind to the inner diameter of the nanotubes. There is still much promise for bR as a bio-photosensitizer because studies have shown that it has nearly twice the absorbance of the traditionally used Ru dye. Reducing the size of the bR membrane fragment will allow for a higher protein loading of the DSSC.

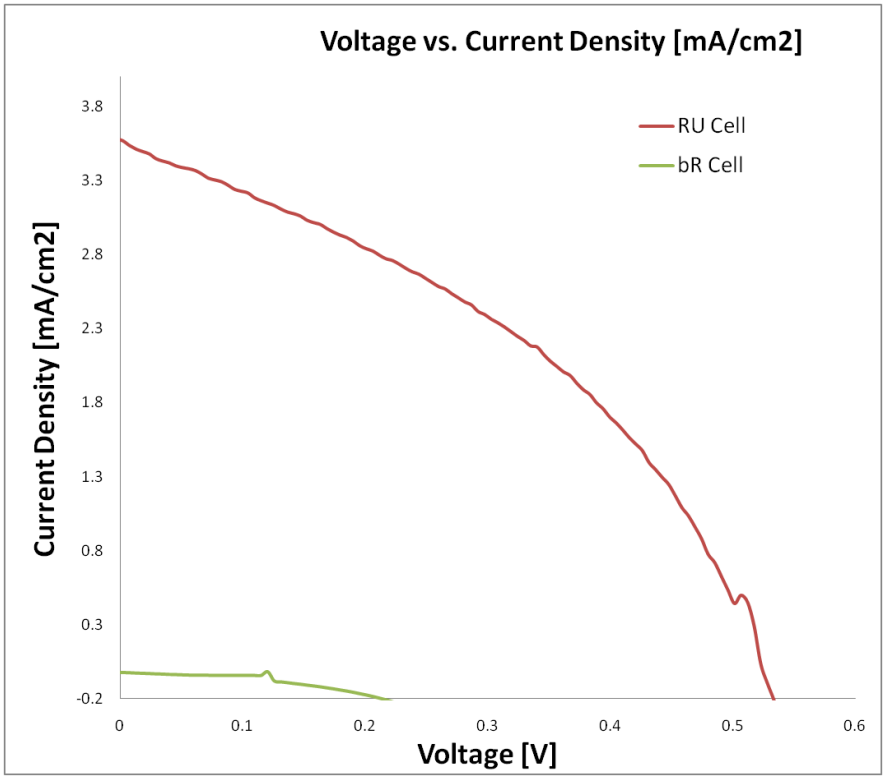

Figure 18. I-V density of a DSSC using Ru-dye vs. a DSSC using bR.

3.4 Size-Controlled Engineering of Bacteriorhodopsin

The bR molecule is a membrane protein, thus is integrated with its associated lipids in a PM fragment form. The PM solution was analyzed via dynamic light scattering (DLS) techniques, shown in figure 19, which reveals the membrane size to be approximately 470 nm in dimension.

These large dimensions will inhibit the integration of bR into the TiO_2 nanotube or nanoparticle substrates.

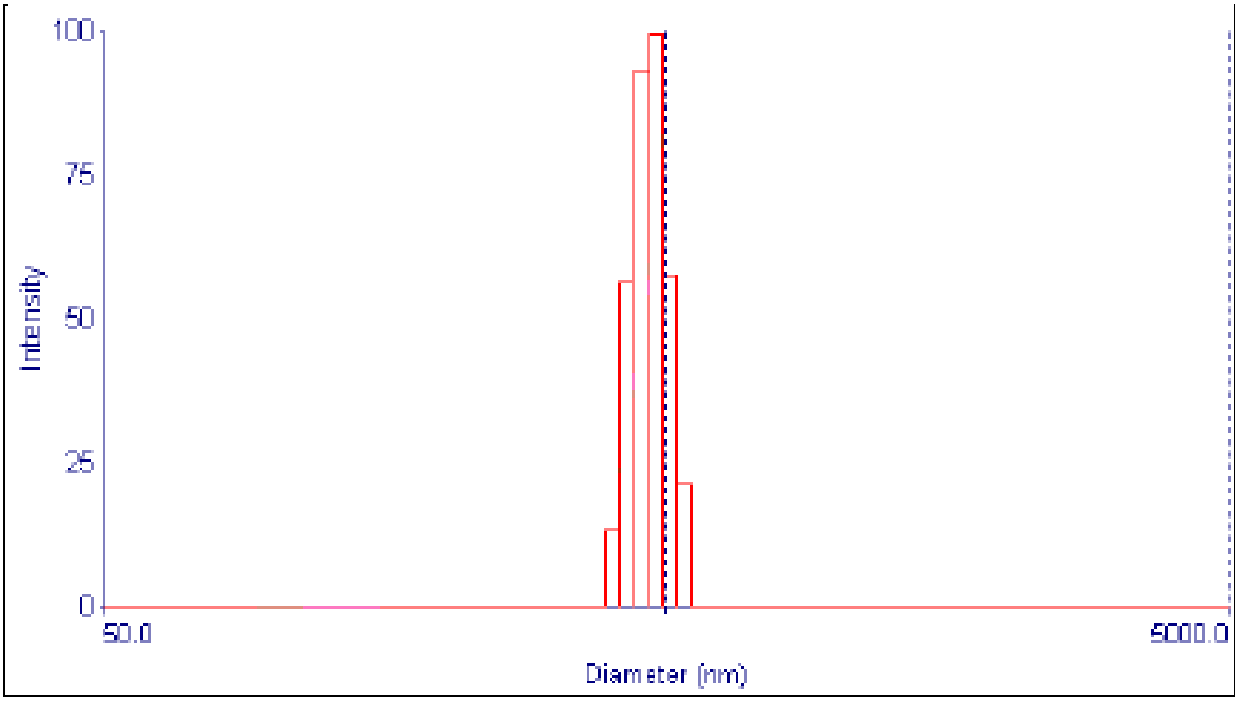

Figure 19. Particle size analysis of PM fragments showing an average fragment diameter of 497.6 nm with a size range of 399.3–536.4 nm.

In order for bR to penetrate the pores of TiO_2 nanotubes, the PM fragment dimensions can be reduced through a detergent dilapidation process. Solubilization of bR can be accomplished by a variety of surfactants, with octyl-β-d-glucopyranoside (OG) selected due to its demonstrated ability to resist denaturing of the bR molecule. As bR uses lipids as scaffolding, care should be placed into maintaining the correct ratio of bR to OG so that bR does not lose the entirety of its lipids, and therefore, its function.

Solutions of varying concentrations of OG were prepared in a phosphate buffer of pH 7.20 to test PM delipidation at OG concentrations ranging from 70 to 275 mM. In order to check if the PM fragments were delipidized, the micro-ultracentrifuge was used to see if a pellet formed. The vials were placed in the centrifuge at 40,000g for 1 h at 23 °C. The larger PM fragments were pelleted out, with the smaller delipidized PM fragments remaining in solution. If no pellet was found, that signaled that the bR had been fully solubilized. Delipidation of the PM fragments is monitored through ultraviolet (UV)-visible (Vis) analysis of the 280:570 nm absorption peak ratio over a 24-h time span. Concentrations of 70, 90, 100, 140, 170, 200, 240, and 275 mM were tested, with the 140 and 170 nM showing the maximal solubilization percentage with the least amount of denaturation. The DLS methodology was used to determine the engineering PM fragment dimensions at OG concentrations 140 and 170 mM, as shown in figure 20.

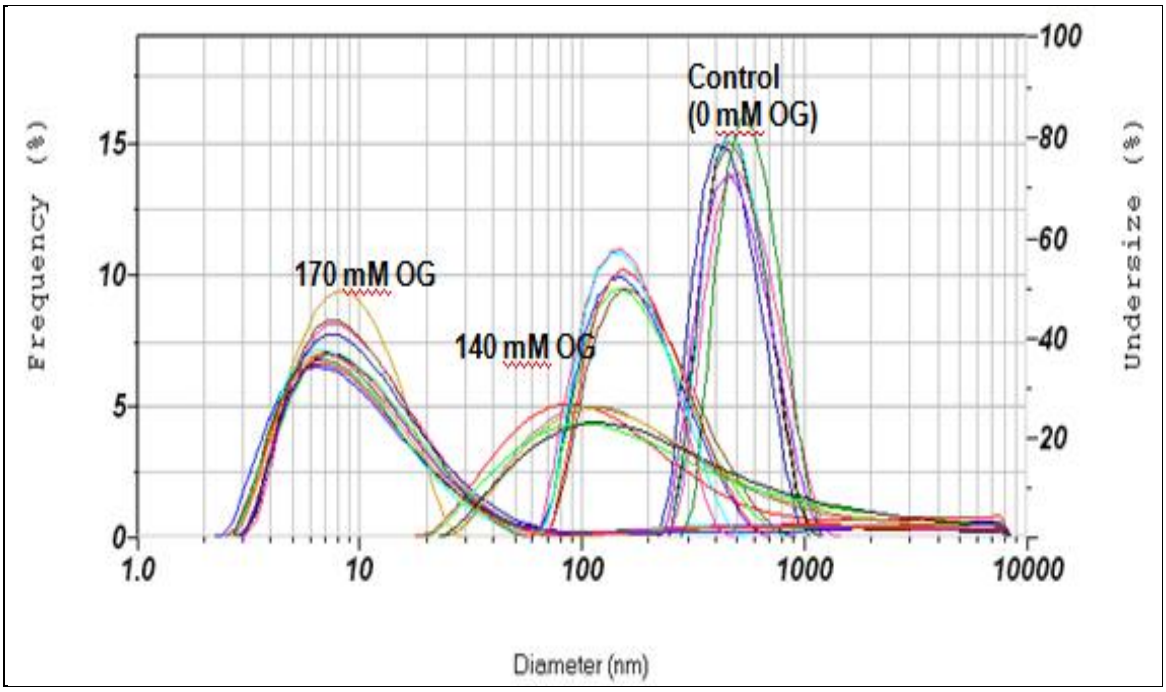

Figure 20. Average diameters of OG concentrations 140 and 170 mM, and the control of 0 mM.

The DLS particle analyzer found the control to have a mode diameter of 453.7 nm, while 140 mM yielded an average particle diameter of 161.2 nm, and the concentration of 170 mM was found to produce an average PM dimensions of 7.6 nm, suggesting complete solubilization. Using the reduced dimensionalities of the bR solution produced through the detergent solubilization technique, the bR is optimized for integration into the DSSC device and can be tailored to the specific nanotube dimensionalities.

4. Conclusion

This study presents a method of obtaining free-standing, highly organized TiO_2 arrays for use in flexible DSSCs. Free-standing, highly oriented and hexagonally packed nanotubes were synthesized and integrated with bR. Future efforts will be directed towards better understanding the growth mechanisms of the TiO_2 nanotube arrays, specifically with bamboo-like rings, with the goal of being able to further control nanotube growth. Combining the nanotubes with an ITO-coated PET using a sol-gel consisting of Ti nanoparticles with be applied in future research and should greatly increase the performance of the solar cell. In order to improve the reported results, a higher concentration of NH_4F within the electrolyte solution should be used to increase the pore size, and experimentation with delipidated bR will be conducted to allow for better integration with TiNT due to a more effective dye-sensitization. Furthermore, the binding mechanism of bR to the surface of the TiO_2 also needs to be investigated. The effects of

performing a carbodiimide linker may possibly bind the bR to the surface of the TiO_2 nanotubes more effectively than traditional dye soaking. This could potentially increase the surface density, thereby increasing the potential of bR as a sensitizer. Finally, it is also important to note that although the nanograss and honeycomb structures grown in this study may not be ideal for use in a DSSC, they could be potentially useful for applications such as bacteria filters, bio-sensors, and various other biomedical applications.

5. References

1. Kang, M. G.; Park, N.-G.; Ryu, K. S.; Chang, S. H. 2001, p. 7.
2. Grätzel, M. *Inorg. Chem.* **2005**, *44*, 6841.
3. Jennings, J. R.; Ghicov, A. *J. Am. Chem. Soc.* **2008**, *130*, 13364–13372.
4. Chiba, Y.; Islam, A.; Watanabe, Y.; Komiya, R.; Koide, N.; Han, L. *Jpn. J. Appl. Phys*. **2006**, *45*, L638.
5. Koops, S. E.; O'Regan, B. C.; Barnes, P.R.F.; Durrant, J. R. *J. Am. Chem. Soc*. **2009**, *131*, 4808.
6. Nelson, J. *Phys. Rev. B: Condens. Matter Mater. Phys.* **1999**, *59*, 15374, LP.
7. Shankar, K.; Mor, G. K.; Prakasam, H. E.; Varghese, O.K.; Grimes, C. A. *Lamg,ior* **2007**, *23*, 12444–12449.
8. Zhu, K.; Neale, N. R.; Miedaner, A.; Frank, A. J. *Nano Lett.* **2007**, *7*, 69–74
9. Ghicov, Andrei; Albu, Sergiu. *Chem. Asian J.* **2009**, *4*, 520–525.
10. Elsanousi, A.; Zhang, J. *J Mater Sci* **2008**, *43*, 7219–7729.
11. Cai, Q.; Paulose, M.; Varghese, O. K. *J Mater Res* **2005**, *20*, 230.
12. Macak, J. M.; Taveroa, L. V.; Tsuchiya, H.; Sirotna, K.; Macak, J.; Schumuki, P. *J Electroceram, 16*, 29.
13. Mor, G. K.; Carvalho, M. A.; Varghese, O. K.; Pisho, M. V.; Grimes, C. A. *J Mater Sci* **2004**, *19*, 628.
14. Prakasam, H. E.; Shankar, K.; Paulose, M.; Varghese, O. K.; Grimes, C. A. *J. Phys. Chem* **2007**, *111*, 7235–7241.
15. Lei, B.; Liao, J.; Zhang, R.; Wang, J.; Su, C.; Kuang, D. *J. Phys. Chem.* C **2010**, *114*, 15528–33.
16. Park, N. G.; Frank, A. J. *J. Phys. Chem. B* **2000**, *104*, 8989–8994.
17. Yang, D. J.; Kim, H. G.; Cho, S. J.; Choi, W. Y. *Mater Lett* **2008**, *62*, 775.
18. Macak, J. M.; Tsuchiya, H.; Ghicov, A.; Yashuda, K.; Schumuki, P. *Curr Opin Solid State Mater Sci* **2007**.

19. Pappas, D. D.; Bujanda, A. A.; Orlicki, J. A.; Jensen, R. E. *Surface and Coatings Technology* **2008**, *203*, 830–834.

20. Borcia, G.; Anderson, C. A.; Brown, N.M.D. *Applied Surface Science* **2004**, *225*, 186–197.

21. Borcia, G.; Anderson, C. A.; Brown, N.M.D. *Applied Surface Science* **2004**, *221*, 203–214.

22. Briggs, D. *Surface Analysis of Polymers by XPS and Static SIMS*; Cambridge University Press: Cambridge, 1998.

23. Gonzalez II, E.; Hicks, R. F. *Langmuir* **2010**, *26*, 3710–3719.

6. Transitions

The technologies developed in this first-year DRI project are being transitioned into the Bio-Nano work package at ARL-WMRD and opportunities for mission funding are being explored. Specific focuses for continued work include further study on the enhanced uptake of bR into the DSSC device and also optimizing the gel polymer electrolyte, sensitizers, and electrodes towards enhanced durability for extreme environments.

List of Symbols, Abbreviations, and Acronyms

1-D	one-dimensional
3-D	three-dimensional
Al	aluminum
Al_2O_3	aluminum oxide
AM	air mass
APC	atmospheric plasma system
ARL	U.S. Army Research Laboratory
bR	bacteriorhodopsin
CCD	charge-coupled device
DBD	dielectric barrier discharge
DI	deionized
DLS	dynamic light scattering
DSSCs	dye-sensitized solar cells
F^-	fluorine ions
FTO	fluorine-doped tin oxide
He	helium
HF	hydrogen fluoride
HOMO	highest occupied molecular orbital
I	iodine
I_3^-	tri-iodide
ITO	indium tin oxide
I-V	current-voltage
LiI	lithium iodide
LUMO	lowest unoccupied molecular orbital

MLCT	metal-to-ligand charge transfer
N_2	nitrogen
NH_4F	ammonium fluoride
O^{2-}	oxygen ions
OG	octyl-β-d-glucopyranoside
PEG	polyethylene glycol
PET	polyethylene terephthalate
PM	purple membrane
Pt	platinum
PTFE	polytetrafluoroethylene
PV	photovoltaic
Ru	ruthenium
SEM	scanning electron microscopy
Si	silicon
Ti	titanium
Ti^{4+}	titanium ions
TiNT	TiO_2 nanotube
TiO_2	titanium dioxide
UHMWPE	ultra-high molecular weight polyethylene
UV	ultraviolet
Vis	visible
WCA	water contact angle
XPS	x-ray photoelectron spectroscopy
XRD	x-ray diffraction

NO. OF COPIES	ORGANIZATION
1 ELEC	ADMNSTR DEFNS TECHL INFO CTR ATTN DTIC OCP 8725 JOHN J KINGMAN RD STE 0944 FT BELVOIR VA 22060-6218
3	US ARMY RSRCH LAB ATTN IMNE ALC HRR MAIL & RECORDS MGMT ATTN RDRL CIO LL TECHL LIB ATTN RDRL CIO LT TECHL PUB ADELPHI MD 20783-1197
5	US ARMY RSRCH LAB ATTN RDRL WMM A MARK GRIEP VICTOR RODRIGUEZ-SANTIAGO ANDRES A. BUJANDA JOSH MARTIN DAPHNE D. PAPPAS APG MD 21005-5069
10	US ARMY RSRCH LAB ATTN RDRL WM SHASHI KARNA APG MD 21005-5069

INTENTIONALLY LEFT BLANK.